748. Design of a magnetostrictive sensor for structural health monitoring of non-ferromagnetic plates

Li Zhou[1], Yajie Yang[2], Fuh-Gwo Yuan[3]
[1, 2] State Key Laboratory of Mechanics and Control of Mechanical Structures
Nanjing University of Aeronautics and Astronautics, No. 29 Yudao Street, Nanjing 210016, China
[3]Department of Mechanical and Aerospace Engineering
North Carolina State University, Raleigh, NC 27695-7921, USA
E-mail: [1]*lzhou@nuaa.edu.cn*, [2]*yjyang804@hotmail.com*, [3]*yuan@ncsu.edu*
(Received 7 December 2011; accepted 14 February 2012)

Abstract. In this work, a magnetostrictive sensor (MsS) is designed and tested for monitoring damage in a non-ferromagnetic plate. Firstly, the mechanism of the MsS to generate and detect guided shear horizontal (SH) waves in a non-ferromagnetic plate is described. Both theoretical and experimental studies are conducted in order to prove that the sensor can generate the first non-dispersive shear horizontal wave mode (SH_0) suitable for monitoring of the structural health. The sensor encompasses a nickel strip, a pair of permanent magnets, C-shaped cores wound by a figure-of-eight coil. The incident wave emitted from the MsS propagates in the plate and is reflected from the plate boundaries. Since the time of the arrival can be determined from the reflected wave signal through signal processing, the velocity of the wave can be extracted. Comparing the calculated velocity with the velocity predicted by the theory, the mode of the wave can be identified with a priori knowledge of plate velocity. To demonstrate the effectiveness of the proposed sensor for structural health monitoring, the location of the damage in an aluminum plate is examined. Finally, optimum design of the sensor is determined using ANSYS program yielding improved sensor performance. The effectiveness of the optimized magnetostrictive sensor is confirmed by experimental results.

Keywords: magnetostriction sensor, ultrasonic stress wave, structure health monitoring, optimization design.

1. Introduction

Ultrasonic guided waves are being used extensively for rapidly detecting the damage in structural health monitoring. Current available sensors for generating/receiving high frequency waves are mainly based on piezoelectricity phenomenon. Recently, magnetostrictive sensors for this purpose have received much attention because of several potential advantages such as non-contact detection and cost-effectiveness [1-4]. Magnetostrictive sensor utilizes the magnetomechanical coupling phenomena between a magnetic field and mechanical deformation based on magnetostriction that can occur in ferromagnetic materials. However, since the magnetostriction occurs only in ferromagnetic materials, most of the applications of the magnetostrictive sensor are limited to ferromagnetic materials. In order to extend its use for any type of material for structural health monitoring, Kwun and his colleagues proposed a magnetostrictive sensor employing a nickel strip as a ferromagnetic patch and bonded it to non-ferromagnetic plates [7, 10, 11].

Using guided waves for monitoring the plate-like structure, the first mode of SH waves (SH_0) is preferred because it is non-dispersive. Thus, proper control of the wave mode and frequency are very critical for the sensor design [7, 12, 17, 18]. The aim of the work is concerned with the development of a magnetostrictive sensor generating and receiving SH_0 wave for structural health monitoring in a non-ferromagnetic plate. The magnetostrictive sensor consists of a nickel strip, permanent magnets (Nd-Fe-B), C-shaped cores and figure-of-eight coils wrapped around two short legs lengthwise. Based on magnetostrictive effect, the active sensor generates guided wave propagating in the plate and the wave is reflected from the damages, boundaries, and

structural features. Since the time of the arrival can be determined from the reflected wave signal received by the MsS through signal processing, the velocity of the wave can be extracted. Comparing the calculated velocity with the velocity predicted by the model, the mode of the wave can be identified with a priori knowledge of velocity of the plate. To demonstrate the effectiveness of the proposed sensor for structural health monitoring, the MsS is applied to identify the location of the damage in an aluminum plate.

Improving sensor performance is always desirable for sensor design. Kim, et al. used a topology optimization method to find the optimal yoke configuration for increasing the sensor signal output [6]. In this investigation, based on the proposed sensor design, magnetic field is the main physical parameter to actuate and sense ultrasonic waves, and the sensor performance is most significantly influenced by the magnetic field in the strip, thus the sensor signal output can be improved if stronger magnetic flux passes through the strip. The objective of this study is to find an optimal magnetic core configuration maximizing the magnetic flux density in the strip by using ANSYS program, which will increase the sensor signal output. The effectiveness of the optimized magnetostrictive sensor is demonstrated by experimental studies.

2. Theoretical background

2. 1 Magnetostriction

Magnetostriction, including both Joule effect and Villari effect, refers to the coupling phenomenon between mechanical deformation and magnetic field change in ferromagnetic materials. Joule effect, also called direct magnetostrictive effect, refers to the phenomenon of the dimension change of the ferromagnetic material when it is placed under a magnetic field. Villari effect, known as the inverse magnetostrictive effect, refers to that when time-varying mechanical loads are applied to ferromagnetic material, the magnetic field distribution within the material changes. The Joule effect and the Villari effect may be expressed in three-dimensions by the following two equations [3]:

Direct magnetostrictive effect
$$\varepsilon_p = s_{pq}^H \sigma_q + q_{pk}^* H_k \tag{1}$$

Converse magnetostrictive effect
$$B_i = q_{iq} \sigma_q + \mu_0 \mu_{ik}^\sigma H_k \tag{2}$$

where $p,q = 1,\ 2,\ \cdots,\ 6;\ i,k = 1,\ 2,\ 3,$ σ_q and ε_p the components of the stress and engineering strain respectively, s_{pq}^H is a component of the compliance matrix at a constant magnetic field. B_i and H_k represent the components of magnetic flux density and magnetic density, respectively. μ_0 (= $4\pi\times10^{-7}$ H/m) is the free-space permeability and μ_{ik}^σ is the normalized permeability tensor at a constant stress field; q_{pk}^* and q_{iq} denote the coupling coefficient of the Joule effect and the Villari effect, respectively.

2. 2 Guided waves in a plate

Conventional ultrasonic techniques are very time-consuming for the inspection of plate-like structures since the sensor must be scanned point-by-point over the whole structural area to be inspected. Guided wave inspection is an emerging technology for rapidly assessing the structural damage. Guided waves refer to elastic waves in ultrasonic and sonic frequencies that propagate in a bounded medium parallel to the plane of its boundary. Guided waves have the potential to be used for the long range inspection of the plate since they can propagate a long distance along the plate and a large region can therefore be interrogated for each sensor position. However, the guided waves are often dispersive; that is, the velocity of the guided

waves varies with the wave frequency and the material and geometry of the medium. This phenomenon is called the dispersion of the guided wave. In addition, at a given wave frequency, the guided waves can propagate in different wave modes. Although the properties of the guided waves are complex, with judicious selection and proper control of wave mode and frequency the guided waves can be very suitable for inspecting structures. In thin plates, guided waves exist in two wave modes: the Lamb waves for both anti-symmetric (A) and symmetric modes (S) and shear horizontal SH waves. Fig. 1 shows the group velocity dispersion curve of guided wave in isotropic plates with $\nu = 0.33$. The group velocity and frequency are normalized by the transverse bulk transverse (shear) velocity $c_T = \sqrt{\nu/\rho}$ and c_T and thickness of the plate, h, respectively. The first SH mode, denoted by SH_0, is a non-dispersive because its group velocity is constant regardless of the frequency. Potential advantages of SH waves compared to the Lamb wave for non-destructive evaluation (NDE) include lower mode conversion, constant wave velocity for the first SH wave mode for all the frequencies.

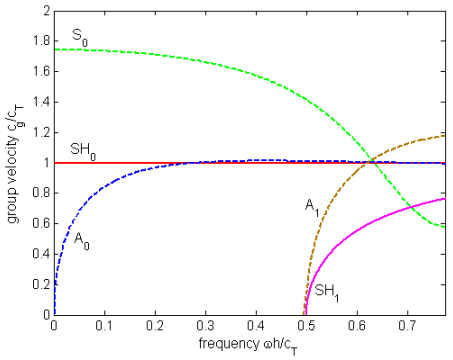

Fig. 1. Calculated dispersion group velocity curves for Lamb wave and SH wave modes of isotropic plates with Poisson ratio, $\nu = 0.33$

3. Sensor design

Kwun and Kim proposed a nickel-patch magnetostrictive sensor for generating and receiving ultrasonic guided waves in non-ferromagnetic materials [12]. Kim developed an orientation-adjustable patch-type magnetostrictive sensor for plates [5]. These sensors generate Lamb waves, which are dispersive and such waves generally require additional efforts for signal processing in damage detection. Due to the non-dispersive nature of the SH_0 wave, such wave is preferred for simplifying the signal processing used for detecting damage in monitoring structural health in a plate. In this work, based on Joule effect and Villari effect, a small, and simple magnetostrictive sensor (MsS), which generates and receives SH wave for structural health monitoring in non-ferromagnetic plates, is introduced. The MsS can be used for both actuator and sensor and it consists of a nickel strip, a pair of permanent magnets (Nd-Fe-B), a C-shaped core made of ferrites and many turns of figure-of-eight coils (i.e. a kind of coil whose figure just like the Arabic numerals '8') wound two short legs lengthwise, as shown in Fig. 2. Because the aluminum plate under inspection is non-ferromagnetic and thus does not exhibit magnetostrictive effect, a nickel strip, which has magnetostrictive effect bonded to the surface of the plate with epoxy is used as the "bridge" to introduce the magnetomechanical coupling into the aluminum plate [5]. First, the nickel strip is magnetized by a constant bias magnetic field perpendicular to the direction of the sensor width supplied by a pair of permanent magnets, and the magnitude of the magnetic flux density is about 3500 Gausses (Gs). When an electrical current pulse is applied to the figure-of-eight coil of the sensor, the coil generates a time-varying magnetic field parallel to the direction of the sensor width, which results in the

dimensional changes caused by the magnetostriction stress in the nickel strip via the Joule effect [3]. The induced dimensional change on the nickel strip, in turn, causes the deformation of the non-ferromagnetic plate and generates guided wave propagating along the plate.

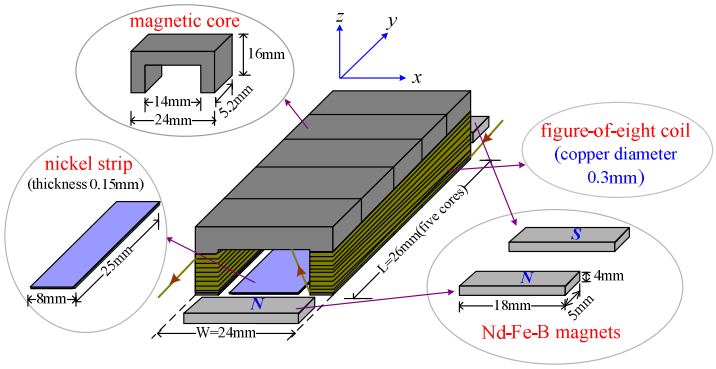

Fig. 2. The dimension and geometry of a magnetostrictive sensor with nickel strip, permanent magnets, cores and figure-of-eight coil

Since the forces induced by the magnetostriction govern the mode of the generated wave, calculating the forces based on the MsS configuration shown in Fig. 2 is determined herein. Based on Joule effect defined as Eq. (1), the magnetostriction stress applied to the plate can be defined as:

$$\sigma_n = -c_{np} q_{pk}^* H_k \tag{3}$$

where $n, p = 1, 2, \ldots, 6$; $k = 1, 2, 3$, σ_n is a component of the magnetostriction stress, c_{np} is the elastic-stiffness coefficient, H_k is magnetic field intensity and q_{pk}^* is the coupling coefficient of the Joule effect which can be written as:

$$q_{pk}^* = \frac{\partial \varepsilon_p}{\partial H_k} \tag{4}$$

The induced magnetostriction stress from the MsS sensor can be considered as body forces in the equations of motion:

$$\begin{aligned} f_x &= \frac{\partial \sigma_x}{\partial x} + \frac{\partial \tau_{xy}}{\partial y} + \frac{\partial \tau_{xz}}{\partial z} \\ f_y &= \frac{\partial \tau_{xy}}{\partial x} + \frac{\partial \sigma_y}{\partial y} + \frac{\partial \tau_{yz}}{\partial z} \\ f_z &= \frac{\partial \tau_{xz}}{\partial x} + \frac{\partial \tau_{yz}}{\partial y} + \frac{\partial \sigma_z}{\partial z} \end{aligned} \tag{5}$$

When a homogenous static bias magnetic field, H_y^0, supplied by a pair of Nd-Fe-B permanent magnets is applied along the *y* direction parallel to the surface in the nickel strip, the longitudinal magnetostriction $\varepsilon(H_y^0)$ appears along the *y*-direction. The magnetostriction along the *x*-direction will be $-v\varepsilon(H_y^0)$ due to the Poisson's effect. Thus the time-independent strain field ε^0 caused by the permanent magnets is

$$\varepsilon_y^0 = \varepsilon(H_y^0), \quad \varepsilon_x^0 = \varepsilon_z^0 = -v\varepsilon(H_y^0), \quad \gamma_{yz}^0 = \gamma_{xz}^0 = \gamma_{xy}^0 = 0. \tag{6}$$

The coupling coefficients related to the field along the *y* direction are therefore given by

$$q_{22}^* = \frac{\partial \varepsilon_y}{\partial H_2} \equiv \gamma, \quad q_{12}^* = q_{32}^* = -\nu\gamma, \; q_{42}^* = q_{52}^* = q_{62}^* = 0 \tag{7}$$

where γ denotes the slope of the magnetostriction curve (bias field versus magnetostriction) and can be measured from experiments.

When the figure-of-eight coil is excited by a time-varying current, it works just like a pair of magnets which are placed at the each side of the nickel strip with opposite poles and thus generates a time-varying magnetic field H_x across nickel strip along the *x* direction. This time-varying magnetic field disturbs the static strain field. Components of the coefficients related to the time-varying magnetostriction can be calculated as follows. When the time-varying field H_x is added, the total field ($H_x\mathbf{i} + H_{0y}\boldsymbol{j}$) occurs along the direction inclined by an angle θ clockwise from the *y* axis and the principal strains arise along the directions parallel and normal to the total field. Thus, in the coordinate system where the y' axis is along the total field, the strains can be expressed as

$$\varepsilon_{y'} = \varepsilon(H_t) \equiv \varepsilon_t, \quad \varepsilon_{x'} = \varepsilon_{z'} = -\nu\varepsilon(H_t) = -\nu\varepsilon_t \tag{8}$$

where $H_t = \sqrt{H_x^2 + H_y^{0^2}}$. The strain field in the original coordinate system takes the form

$$\begin{aligned}
&\varepsilon_x = \varepsilon_{x'}\cos^2\theta + \varepsilon_{y'}\sin^2\theta \\
&\varepsilon_y = \varepsilon_{y'}\cos^2\theta + \varepsilon_{x'}\sin^2\theta \\
&\varepsilon_z = \varepsilon_{z'} \\
&\tau_{yz} = \tau_{xz} = 0 \\
&\tau_{xy} = (\varepsilon_{y'} - \varepsilon_{x'})\sin 2\theta = (1+\nu)\varepsilon_t \sin 2\theta
\end{aligned} \tag{9}$$

Then we have

$$\begin{aligned}
q_{11}^* &= \frac{\partial}{\partial H_x}(\varepsilon_{x'}\cos^2\theta + \varepsilon_{y'}\sin^2\theta) \\
&= \frac{2(1+\nu)\varepsilon_t}{H_y^0}\cos^3\theta\sin\theta + \gamma\sin\theta(-\nu\cos^2\theta + \sin^2\theta), \\
q_{21}^* &= -\frac{2(1+\nu)\varepsilon_t}{H_y^0}\cos^3\theta\sin\theta + \gamma\sin\theta(-\nu\sin^2\theta + \cos^2\theta), \\
q_{31}^* &= -\nu\gamma\sin\theta, \\
q_{61}^* &= (1+\nu)\gamma\sin 2\theta\sin\theta + \frac{2(1+\nu)\varepsilon_t}{H_y^0}\cos^2\theta\cos 2\theta
\end{aligned} \tag{10}$$

Following the same approach, the coefficients relating to H_z can be shown as:

$$q_{13}^* = q_{31}^*, \; q_{23}^* = q_{21}^*, \; q_{33}^* = q_{11}^*, \; q_{43}^* = q_{61}^*, \; q_{53}^* = q_{63}^* = 0 \tag{11}$$

At high static bias fields $H_y^0 >> H_x$ and H_z ($\sin\theta \approx 0$), the matrix q_{pk}^* takes the following form for the bias field:

$$\left[q_{pk}^{*}\right]=\begin{bmatrix} 0 & -\nu\gamma & 0 \\ 0 & \gamma & 0 \\ 0 & -\nu\gamma & 0 \\ 0 & 0 & \dfrac{2(1+\nu)\varepsilon_t}{H_y^0} \\ 0 & 0 & 0 \\ \dfrac{2(1+\nu)\varepsilon_t}{H_y^0} & 0 & 0 \end{bmatrix} \tag{12}$$

Considering the stress-free condition and the isotropic nickel strip, Eq. (3), Eq. (5) and Eq. (12) are combined to derive the body forces caused by the magnetostriction stress as:

$$f_x = f_z = 0$$

$$f_y = \frac{\partial \tau_{xy}}{\partial x} = -\frac{2(1+\nu)\varepsilon_t G}{H_y^0}\frac{\partial H_x}{\partial x}, \tag{13}$$

where H_y^0 is the magnetic field supplied by a pair of Nd-Fe-B permanent magnets, H_x is the time-varying magnetic field caused by the coil, G is shear modulus of the nickel strip and ε_t is the magnetostriction of the nickel which can be measured [2, 3]. As can be seen from Eq. (13), the nonzero body forces occurs only in the *y* direction in this configuration, this MsS sensor can generate SH shear waves propagating in the *x* direction with polarization along the *y* direction.

The guided waves propagate along the plate and are reflected from the boundaries of the plate. Based on the Villari effect, the stress wave developed in the nickel strip will alter its magnetic state and the resulting magnetic flux Φ enclosed by the coil of the sensor can be measured by the Faraday-Lenz law to give the voltage change V [19]:

$$V = -\frac{d\Phi}{dt} = -\frac{Nd\varphi}{dt} \tag{14}$$

where t is the time, N is the number of the coil turns of the sensor, and φ is the magnetic flux encircled by a single turn of the coil. The magnetic flux φ is an integral of the magnetic flux density B over the cross-sectional area enclosed by the coil.

4. Experiments

4. 1 Experimental arrangement

An aluminum plate with dimension 500×200×3 mm, as shown in Fig. 3, is used for testing the proposed MsS. The material properties of the aluminum are: Young's modulus E = 80GPa, ν = 0.33 and density ρ = 2.8 g/cm^3. The two MsSs acting as actuator and sensor respectively are located along the middle horizontal *x*-axis of the plate with distance 200 mm apart. The main instruments used in this experiment are NI PXI-5412 Waveform Generator, K-H Model 7602 Power Amplifier, Tektronix TDS3012 Digital Oscilloscope and computer. The coil in the actuator is activated by applying a narrowband voltage signal given by Eq. (15) from a signal generator after amplified by the power amplifier. Then the received signals are displayed by the oscilloscope and analyzed by the computer:

$$V(t) = A[\mathrm{H}(t) - \mathrm{H}(t - n/f_c)](1 - \cos(2\pi f_c t/n))\sin 2\pi f_c t, \tag{15}$$

where A = 120 V is the amplitude modulation of the signal in the following sets of experiments, f_c is the center frequency of the wave, $n = 5$ is the number of the signal cycles and $H(t)$ is Heaviside step function. Fig. 4 shows a typical waveform of the signal with the center frequency of 200 kHz.

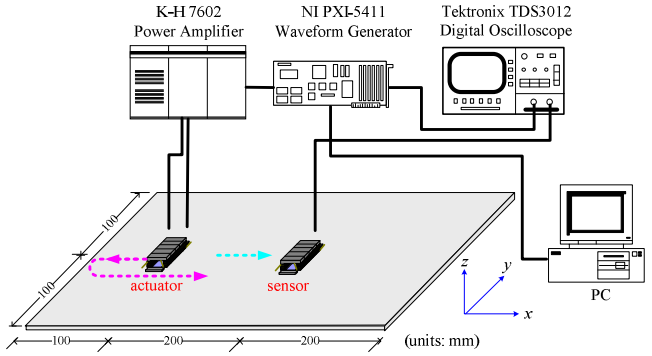

Fig. 3. Experimental setup for SH wave generation and reception on an aluminum plate

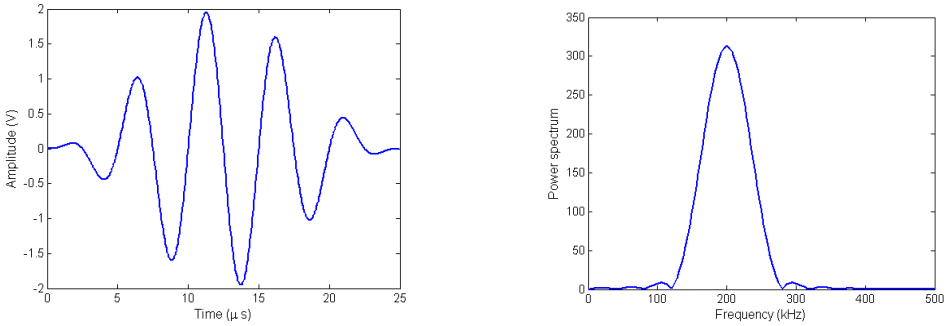

Fig. 4. The excitation signal shown in the time domain with the center frequency of 200 kHz

4. 2 Results and discussion

In this work, the MsS actuator excites the center frequency signals ranging from 100 kHz to 350 kHz with 50 kHz increment. Figs. 5(a) and (b) show the measured signal with excitation frequency at 200 kHz and the corresponding results shown in time-frequency window using Gabor wavelet [20]. As can be observed, the frequency of the detected signals is concentrated approximately around the excited center frequency. The dispersion from the five-peaked signals for the three wave packets shown in Fig. 5(a) may be attributed to the non-uniform hand-wrapping coils around the two short legs of the cores.

It has been proved that the location of the peak on the time-frequency plane indicates the arrival time of the group velocity c_g at frequency $f = 1/a$, where a is the scale [4]. With the measured time difference of the arrival (TDOA) at a certain frequency and the known distance between the actuator and the left boundary of the plate, the group velocity at the corresponding frequency can be determined. Fig. 5(c) shows the 2D plot of the magnitude of Gabor wavelet transform (WT) coefficients at a given scale a (according to $a = f_s/f'$, where f' is a certain frequency at which the group velocity of the wave is calculated, sampling rate f_s = 25 MHz), in which b_1 indicates the arrival time that the wave reaches the sensor from the actuator, b_2 indicates the arrival time that the wave reflected from the left boundary of the plate. Since the distance corresponds to the difference of the two time arrivals, (b_2-b_1), is simply 100×2 = 200

mm, the group velocity of the wave can be calculated as 200 mm/(b_2-b_1), and the calculated velocities at different frequencies, below the cut-off frequency SH_1=500 kHz, are as follows: 3003 m/s at 100 kHz, 3185 m/s at 150 kHz, 3175 m/s at 200 kHz, 3180 m/s at 250 kHz, 3135 m/s at 300 kHz, 3125 m/s at 350 kHz. Fig. 6 shows the experimental results for velocity at various frequencies and the dispersion curves. It can be noticed, with different excitation frequencies, that the velocities agree well with the velocity 3100 m/s for SH_0 from the theory. It may be concluded that the proposed magnetostrictive sensor enables reliable generation and reception of SH_0 wave in the non-ferromagnetic plate.

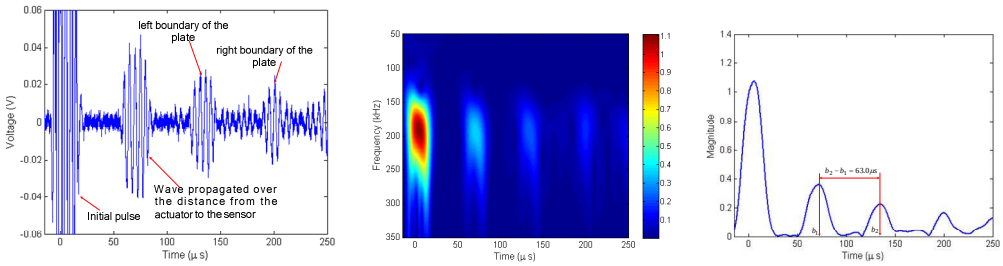

(a) (b) (c)

Fig. 5. The measured signal with the excitation center frequency at 200 kHz (a) in time domain and (b) its Gabor wavelet (c) the magnitude of Gabor wavelet transform coefficient at the corresponding excitation frequency

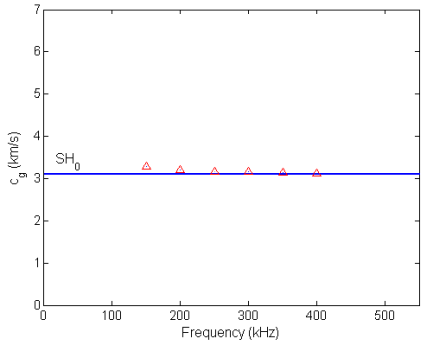

Fig. 6. Calculated velocities at different excitation frequencies: line - theoretical data; triangles - experimental data

4. 3 Damage detection

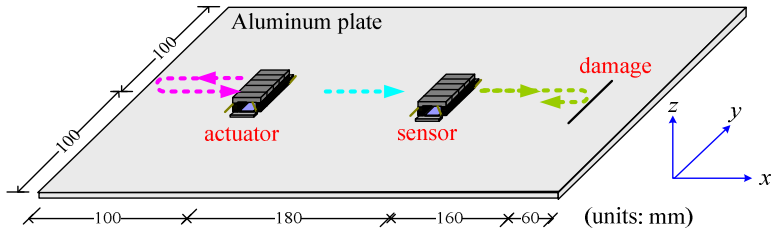

Fig. 7. A pair of magnetostrictive sensors for locating the damage in an aluminum plate

To demonstrate the effectiveness of the proposed sensor for structural health monitoring, a pair of magnetostrictive sensors are applied to locate the damage in an aluminum plate using the same experimental setup as that in the previous study. The illustration of the test plate with

damage and a pair of magnetostrictive sensors is shown in Fig. 7. The test structure is also a 3 mm thick aluminum plate. The thickness-the-thickness damage about 30 mm in length, 0.5 mm in width is made on the plate about 160 mm away from the sensor. The waveform generator generates a narrowband voltage signal with center frequency of 250 kHz. Then the signal is applied to the transmitting coils, which generates SH_0 wave in the plate. As shown in Fig. 7, the generated wave propagated in both positive and negative *x*-directions and reflected by the damage and the boundaries of the plate. Fig. 8(a) shows the signals received by the sensor. It can be seen from the figure, the third wave packet is the signal solely from the damage. Gabor wavelet transform is applied to the received scattered signals from the damage in the time-frequency domain to extract the characteristic information such as time arrival, as shown in Fig. 8(b), Fig. 8(c) shows the magnitude of Gabor WT coefficient at the corresponding excitation frequency at 250 kHz, where b_1 indicates the arrival time that the wave reaches the sensor from the actuator, b_2 indicates the time arrival that the wave reflected from the damage. Since the SH_0 wave velocity is 3100 m/s, the distance corresponds the section time (b_2-b_1) can be calculated as 3100×(b_2-b_1) = 317.8 mm, and then the distance between the sensor and damage is 317.8/2 = 158.9 mm, which agrees well with the actual distance (160 mm). As can be seen, the proposed sensor shows its promise in applying in SHM and nondestructive evaluation (NDE).

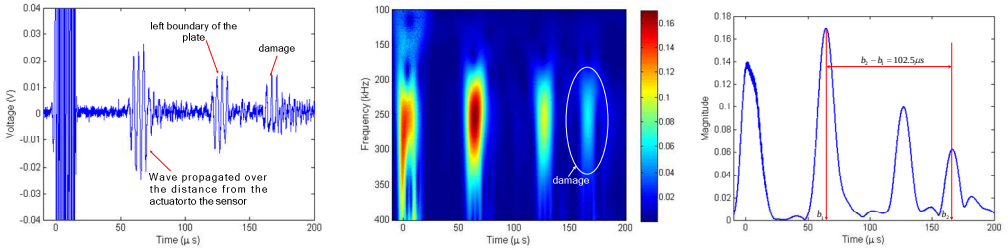

(a) (b) (c)

Fig. 8. The measured scattered signals from the damage with the excitation center frequency at 250 kHz (a) in time domain and (b) its Gabor wavelet (c) the magnitude of Gabor WT coefficient at the corresponding excitation frequency

5. Optimization Design

5. 1 Optimization scheme

Fig. 9(a) shows a schematic of the magnetostrictive sensor configuration encompassing a nickel strip, permanent magnets giving rise to static bias magnetic field and a pair of coils supplying or sensing time-varying field. Eq. (13) denotes the body force induced by the magnetostriction stress. Clearly, the magnetic field H_x is the main physical parameter to actuate and sense ultrasonic waves, and the sensor performance is most significantly influenced by the magnetic field in the strip. However, the magnetic field (equals to the magnetic flux density divided by permeability), thus the sensor signal output can be improved if stronger magnetic flux is generated in the strip. It is natural to consider introducing magnetic cores to the sensor to increase the sensor output under a given magnetic field as in Fig. 9(b), but the output cannot be substantially increased unless the core configuration is optimized, thus the objective of this study is to find optimal magnetic core configuration maximizing the *x* component of the magnetic flux density (B_x) produced by current-flowing coils, and ANSYS program is employed to optimize the design. Note that in Fig. 9(b), the length, width and height of the core are the design variables, and the reciprocal of the total *x* component of the magnetic flux density (B_x) in the elements located in nickel strip multiplied by 10^4 is the objective function for

minimizing the density in ANSYS. The length, width, height and thickness of coils are 28 mm, 11 mm, 8 mm and 2 mm respectively. Fig. 9(c) shows the finite element model used to optimize the core configuration by ANSYS.

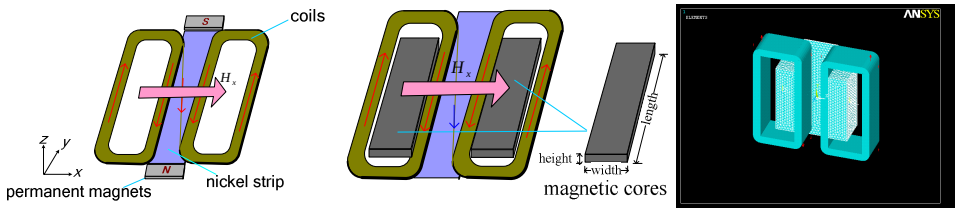

(a) (b) (c)

Fig. 9. (a) Schematic diagram of magnetostrictive sensor. (b) Schematic diagram of cores to be optimized. (c) Finite element model used to optimize cores configuration by ANSYS

5. 2 Numerical results

The initial guesses of the design variables are set as length = 18 mm, width = 5 mm and height = 8 mm. The initial values assigned to these parameters represent a starting design, which is later modified by the optimizer. After design optimization, the best design set is length = 23.7 mm, width = 5.2 mm, height = 18.5 mm. The total x component of the magnetic flux density (B_x) in the elements located in nickel strip increased from the initial 4164.5 Gs to 7926.6 Gs, as can be observed in Fig. 10(a). To better understand the effect of the magnetic cores illustrated in Fig. 9(b) on the magnetic flux density in the strip, a simulation without cores is also performed. Fig. 10(b) shows that the total x component of the magnetic flux density (B_x) in the elements located in nickel strip corresponding to the model without cores is 771.9 Gs. Therefore the optimal cores increase the x component of the magnetic flux density (B_x) in nickel strip dramatically.

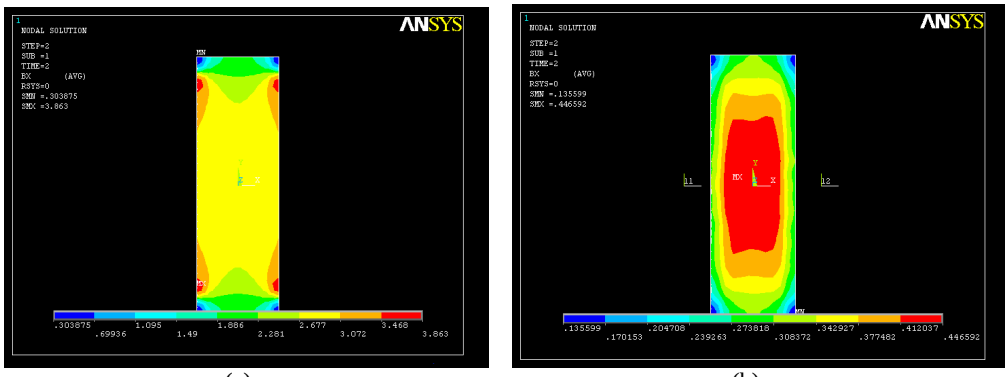

(a) (b)

Fig. 10. The x component of the magnetic flux density (B_x) in the elements located in nickel strip corresponding to (a) the best design set (b) the model without cores

5. 3 Experimental verifications

Fig. 11 illustrates the effects of using the optimum sensor design with optimal magnetic cores on the signal output with the experimental setup shown in Fig. 3. The narrowband excitation signal with the center frequency of f_c = 250 kHz was sent to the actuator while the sensor picked up the wave propagating along the test plate. Note that the top picture in Fig. 11(a) is the signal received by the sensor without magnetic cores, the middle is with the cores before optimization,

and the bottom is for the case of optimized cores. To visualize the improvement on sensor output more clearly, Gabor wavelet transform is applied to the received signals and pick up the Gabor WT coefficient at the corresponding excitation frequency at 250 kHz shown in Fig. 11(b). It can be observed from these figures that the use of the optimal magnetic cores increases the output voltage.

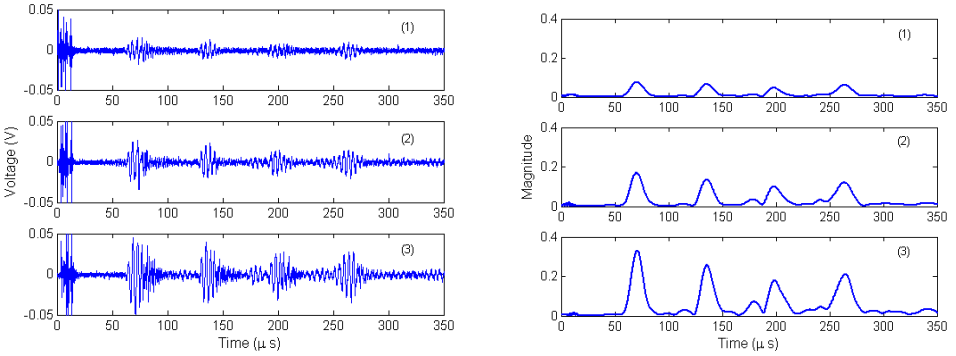

(a) (b)

Fig. 11. (a) The signals received by the sensor (b) the magnitude of Gabor WT coefficient at the corresponding excitation frequency at 250 kHz: (1) without core, (2) with cores prior to optimization, (3) with optimal cores

6. Conclusions

The results of this investigation demonstrate that the proposed magnetostrictive sensor consisting of nickel strips, permanent magnets, two short legs of the C-shaped cores wound by figure-of-eight coils can reliably generate and receive guided SH waves in the non-ferromagnetic plate. Secondly, with different excitation frequencies, the velocities of the guided waves propagating along the plate agree well with the velocity of 3100 m/s for SH_0 waves predicted by the theory. It is confirmed that the proposed magnetostrictive sensor can generate SH_0 wave in the plate. Thirdly, since the mode of the wave excited by the sensor has been known, it can be used for detecting and locating damage in the plate. Finally, the optimized sensor design was established by means of ANSYS. The sensor placed on optimized cores increases the sensor signal output significantly. As the theory of magnetostriction and guided wave inspection technology progress, future active research and development of modeling the MsS to consider all the factors that influence the sensor performance and the relationship between input voltage and output voltage are expected to follow.

Acknowledgments

This work is supported by the Award from National Natural Science Foundation of China (No. 11172128), the Funds for International Cooperation and Exchange of the National Natural Science Foundation of China (No. 61161120323), the Jiangsu Province for Six Kinds of Excellent Talent of China (No. 2010-JZ-004) and Jiangsu Graduate Training Innovation Project (CX09B_070Z).

References

[1] **Balanis Constantine A.** Advanced Engineering Electromagnetics, New York: John Wiley & Sons, 1989, p. 42-95.

[2] Cho S. H., Sun Kim H. W., Kim Y. Y. Megahertz-range guided pure torsional wave transduction and experiments using a magnetostrictive transducer. IEEE Transactions on Ultrasonics, Ferroelectrics and Frequency Control, 57(5), 2010, p. 1225-1229.

[3] Ogi H., Hirao M., Minoura K. Noncontact measurement of ultrasonic attenuation during rotating fatigue test of steel. Journal of Applied Physics, 81(8), 2009, p. 3677-3684.

[4] Jeong H., Jang Y. S. Wavelet analysis of plate wave propagation in composite laminates. Composite Structures, 49, 2000, p. 443-450.

[5] Kim I. K., Cho S. H., Lee J. S., Kim Y. Y. Magnetostrictive grating transducers: effects of grating size and shape. 2005 IEEE Ultrasonics Symposium, 2005, p. 2081-2084.

[6] Kim I. K., Kim W., Kim Y. Y. Magnetostrictive grating with an optimal yoke for generating high-output frequency-tuned SH waves in a plate. Sensors and Actuators A: Physical, 137(1), 2007, p. 141-146.

[7] Lee J. S., Kim Y. Y., Cho S. H. Beam-focused shear-horizontal wave generation in a plate by a circular magnetostrictive patch transducer employing a planar solenoid array. Smart Materials and Structures, 18(1), 2009, p. 1-9.

[8] Calkins F. T., Flatau A. B., Dapino M. J. Overview of magnetostrictive sensor technology. Journal of Intelligent Material Systems and Structures, 18(10), 2007, p. 1057-1066.

[9] Lee J. S., Cho S. H., Kim Y. Y. Radiation pattern of Lamb waves generated by a circular magnetostrictive patch transducer. Applied Physics Letters, 90(5), 2007, p. 054102 - 054102-3.

[10] Kwun H., Bartels K. A. Magnetostrictive sensor technology and its applications. Ultrasonics, 36, 1998, p. 171-178.

[11] Kwun H., Holt A. E. Feasibility of under-lagging corrosion detection in steel pipe using the magnetostrictive sensor technique. NDT&E International, 28(4), 1995, p. 211-214.

[12] Kwun H., Kim S. Y. Magnetostrictive sensor for generating and detecting plate guided waves. Journal of Pressure Vessel Technology, 127(3), 2005, p. 284-289.

[13] Kwun H., Kim S. Y., Light G. M. Long-range guided wave inspection of structures using the magnetostrictive sensor. J. Korean Soc. NDT, 21, 2001, p. 383-390.

[14] Kwun H., Kim S. Y., Light G. M. Magnetostrictive sensor guided-wave probes for structural health monitoring of pipelines and pressure vessels. The 5th International Workshop on Structural Health Monitoring, Stanford University, 2005, p. 694-701.

[15] Kwun H., Light G. M., Kim S. Y., Spinks R. L. Magnetostrictive sensor for active health monitoring in structures. Proceedings of the SPIE - The International Society for Optical Engineering, 4702, 2002, p. 282-288.

[16] Kwun H., Teller C. M. Magnetostrictive generation and detection of longitudinal, torsional, and flexural waves in a steel rod. J. Acoust. Soc. Am., 96(2), 1994, p. 1202-1204.

[17] Murayama R. Study of driving mechanism on electromagnetic acoustic transducer for Lamb wave using magnetostrictive effect and application in drawability evaluation of thin steel sheets. Ultrasonics, 37 (1), 1999, p. 31-38.

[18] Murayama R., Makiyama S., Kodama M., Taniguchi Y. Development of an ultrasonic inspection robot using an electromagnetic acoustic transducer for a Lamb wave and an SH-plate wave. Ultrasonics, 42, 2004, p. 825-829.

[19] Park C. I., Cho S. H., Han S. W., Kim Y. Y. Efficient generation and measurement of guided torsional waves using magnetostrictive nickel patches. Proceedings - IEEE Ultrasonics Symposium, 2, 2004, p. 1290-1293.

[20] Wang L., Yuan F. G. Group velocity and characteristic wave curves of Lamb waves in composites: modeling and experiments. Composites Science and Technology, 67(7-8), 2007, p. 370-1384.